Acta Crystallographica Section D
Biological Crystallography
ISSN 0907-4449

Structure of the α-amylase inhibitor tendamistat at 0.93 Å

Verena König,[a] László Vértesy[b] and Thomas R. Schneider[a]*

[a]Department of Structural Chemistry, University of Göttingen, Tammannstrasse 4, 37077 Göttingen, Germany, and [b]Hoechst Marion Roussel Germany, H780, 65926 Frankfurt/Main, Germany

Correspondence e-mail: trs@shelx.uni-ac.gwdg.de

Received 6 May 2003
Accepted 16 July 2003

PDB Reference: tendamistat, 1ok0, r1ok0sf.

The crystal structure of the proteinaceous α-amylase inhibitor tendamistat has been determined at 100 K to a resolution of 0.93 Å. The final R factor for all reflections with $F > 4\sigma(F)$ is 9.26%. The mean coordinate error for fully occupied protein atoms as derived from full-matrix inversion is 0.018 Å. An extended network of multiple discrete conformations has been identified on the side of tendamistat that binds to the target molecule. Most notably, residue Tyr15, which interacts with the glycine-rich loop characteristic of mammalian amylases, and a cluster of amino-acid side chains surrounding it are found in two well defined conformations. The flexibility observed in this crystal structure together with information about residues fixed by lattice contacts in the crystal but found to be mobile in a previous NMR study supports a model in which most of the residues involved in binding are not fixed in the free form of the inhibitor, suggesting an induced-fit type of binding.

1. Introduction

Tendamistat is a 74-amino-acid protein produced by *Streptomyces tendae*. Although it is not clear what the physiological role of the protein is in the producing organism, tendamistat has been found to be a strong inhibitor targetting a wide range of mammalian α-amylases. This observation evoked considerable interest in the substance as a potential therapeutic in the treatment of diabetes mellitus, as tendamistat could be used to inhibit α-amylases in the human stomach in order to reduce postprandial glucose peaks (Aschauer *et al.*, 1983; Meyer *et al.*, 1984). Unfortunately, tendamistat turned out to be immunogenic. Nevertheless, interest in the molecule continues as a scaffold for the design of related inhibitors and as a model system for biophysical studies on protein folding.

The primary structure of the protein has been defined by Aschauer *et al.* (1983) and the crystal structure of the free inhibitor has been determined to 2.0 Å at room temperature (Pflugrath *et al.*, 1986; PDB code 1hoe). An extensive comparison of this crystal structure with the corresponding structure in solution as determined by NMR (Kline *et al.*, 1988; PDB code 2ait) has been published (Billeter *et al.*, 1989). The close similarity between the NMR structure and the crystal structure was also demonstrated by Braun *et al.* (1989), who showed that a structural model originating from an NMR experiment could be successfully used as a search model for crystallographic phasing *via* molecular replacement. Furthermore, the crystal structure of a complex between porcine pancreatic α-amylase (PAA) and tendamistat has been determined by Wiegand and coworkers to a resolution of 2.5 Å (Wiegand *et al.*, 1995; PDB code 1bvn).

Table 1
Data statistics for tendamistat in space group $P2_12_12_1$ with unit-cell parameters a = 25.68, b = 40.78, c = 60.95 Å, $\alpha = \beta = \gamma = 90.0^\circ$ as determined by post-refinement with *SCALEPACK*.

Values in parentheses are for the highest resolution shell (0.95–0.93 Å, corresponding to 2167 reflections).

Resolution range (Å)	40.0–0.93
No. of observations	261064
No. of unique reflections	41072
Redundancy	6.9 (3.5)
$\langle I/\sigma(I)\rangle$	20.3 (4.3)
Completeness (%)	93.5 (79.9)
$R_{\rm int}$† (%)	5.4 (32.6)

† $R_{\rm int} = \sum(|I - \langle I\rangle|)/\sum I$.

Binding of tendamistat to pig pancreatic α-amylase involves 1330 Å^2 of surface area, corresponding to 30% of the total water-accessible surface area of the free inhibitor molecule, and leads to a steric blockage of the active site of the target molecule (Wiegand *et al.*, 1995), in part explaining the very low inhibition constant (9×10^{-12}; Vértesy *et al.*, 1984). Nevertheless, a detailed understanding of inhibitor binding is necessary to facilitate the design of mimetics of tendamistat as described by Sefler *et al.* (1997) and Ono *et al.* (2001).

In recent years, tendamistat has attracted interest as a model system for molecular-dynamics simulations (*e.g.* Doruker *et al.*, 2000; Bonvin & van Gunsteren, 2000) and the developments of methods and algorithms for protein structure determination by NMR techniques (Gorler & Kalbitzer, 1997; Scarselli *et al.*, 1999). On the experimental side, protein folding (Schonbrunner *et al.*, 1997; Bachmann & Kiefhaber, 2001; Pappenberger *et al.*, 2000, 2003) and protein stability (Balbach *et al.*, 1998) have been studied using tendamistat as a model.

In the following, we report the crystal structure of tendamistat at atomic resolution and discuss a number of aspects that are of importance for understanding its mode of binding to α-amylases.

2. Experimental

2.1. Purification and crystallization

The protein was purified from cultures for *Streptomyces tendae* 4158, ATCC 31210, by adsorption resin and ion-exchange chromatography and crystallization at pH 5 as described by Vértesy *et al.* (1984). All solutions used for crystallization were sterile-filtered and contained 0.03% sodium azide. For crystallization, 20 mg of lyophilized protein was dissolved in 1 ml of double-distilled water. Initial attempts using the crystallization conditions described by Pflugrath *et al.* (1986) employing the batch method were unsuccessful. Using the hanging-drop method with drops consisting of 2 µl protein solution (20 mg ml^{-1}) and 2 µl reservoir solution (0.1–0.5 *M* NaCl adjusted to pH 1.3 with hydrochloric acid) yielded tuft-shaped agglomerates of essentially one-dimensional crystals. Streak-seeding *via* a cat whisker after touching these agglomerates gave single crystals with dimensions of up to 0.1 × 0.01 × 0.01 mm. These single crystals were then extracted using a glass capillary, carefully cleaned in a washing solution (0.2 *M* NaCl pH 1.3) and then transferred into a pre-equilibrated (48 h) 4 µl drop consisting of 2 µl protein solution (20 mg ml^{-1}) and 2 µl reservoir solution (0.15 *M* NaCl pH 1.3). With repeated macroseeding, high-quality crystals with dimensions of up to 1.4 × 0.1 × 0.1 mm that diffracted to atomic resolution were obtained.

2.2. Data collection and processing

For data collection, a crystal was cut to a size of 0.1 × 0.1 × 0.3 using an acupuncture needle and transferred to a storage solution containing 0.2 *M* NaCl pH 1.3. The crystal was then equilibrated with cryosolutions of increasing concentrations of glycerol (in steps of 5%) until a final concentration of 30% glycerol was reached, picked up in a fibre loop (Hampton Research, USA) and flash-cooled in a stream of nitrogen gas at 100 K provided by a home-built cryo-apparatus (Kottke & Stalke, 1993).

Data to 0.93 Å were collected from a crystal at 100 K on beamline X11 (λ = 0.911 Å) at EMBL c/o DESY using a MAR345 imaging-plate scanner. The data collection comprised three passes to limiting resolutions of 0.93, 1.6 and 2.7 Å and took a total of 12 h to collect. Data were integrated and scaled using *DENZO* and *SCALEPACK* (Otwinowski & Minor, 1997). The scaling statistics did not show any sign of radiation damage. Further data analysis and merging was performed using *XPREP* (Bruker AXS, Madison, USA). The resulting data set shows good internal consistency (Table 1). The missing data correspond to data located in the blind region that were not accessible owing to technical problems with the goniometer head. 5% of the unique reflections (2054) were randomly selected with *XPREP* for use in cross-validation.

2.3. Refinement

Starting from the model refined by Huber and coworkers (Pflugrath *et al.*, 1986), the structure was refined against diffraction intensities using the program *SHELXL*97 employing a standard protocol similar to that described by Sheldrick & Schneider (1997). Graphical model building was performed with *XFIT* (McRee, 1999). $R_{\rm free}$ and $R_{\rm work}$ for the best isotropic model were 20.0 and 19.1%, respectively. Inclusion of restrained anisotropic displacement parameters into the refinement led to a drop in $R_{\rm work}$ and $R_{\rm free}$ of 5.5 and 5.6%, respectively. Introduction of discretely disordered side chains, additional fully and partially occupied waters and H atoms (except hydroxyl H atoms) in calculated positions gave values of 9.2% for $R_{\rm work}$ and 11.9% for $R_{\rm free}$ (Table 2) for the best model. Water molecules were modelled in three categories.

(i) Fully occupied sites.

(ii) Networks of partially occupied sites connected either to protein or to at least two other water molecules. If unambiguous assignment to networks was possible, *SHELXL* free variables were used to refine constrained occupancies. Otherwise, the occupancies were set to 0.5.

(iii) Pairs of partially occupied waters.

Table 2
Refinement statistics.

'Full' corresponds to sites with unit occupancy and 'partial' to sites with non-unit occupancy. For partially occupied protein sites (*), the average has been calculated after removal of three outliers with a coordinate uncertainty larger than 1.5 Å. $R1 = \sum \big||F_o| - |F_c|\big| / \sum |F_o|$.

Resolution range (Å)	10.0–0.93
No. reflections	41006
R_{free}/R_{work} [$F_o > 4\sigma(F_o)$] (%)	11.97/9.22
R_{free}/R_{work} (all data) (%)	13.00/10.26
No. of reflections [$F_o > 4\sigma(F_o)$]	35614
$R1$ for $F_o > 4\sigma(F_o)$ (%)	9.26
$R1$ for all data (%)	10.29
No. of parameters	7443
No. of refined non-H sites	
Total (full/partial)	545/282
Protein (full/partial)	463/190
Water (full/partial)	76/83
Others (full/partial)	6/8
R.m.s. deviations from ideal values	
Bond distances (Å)	0.015
Angle distances (Å)	0.033
Planar groups (Å)	0.341
DELU (Å^2)	0.005
SIMU (Å^2)	0.033
ISOR (Å^2)	0.087
Average isotropic B factors	
Protein (full/partial) (Å^2)	7.4/8.7
Water (full/partial) (Å^2)	22.9/18.3
Others (full/partial) (Å^2)	20.6/13.9
Average coordinate uncertainties	
Protein (full/partial*) (Å)	0.018/0.246
Water (full/partial) (Å)	0.044/0.079
Others (full/partial) (Å)	0.054/0.047

In a number of cases, backbone atoms were included in the disordered parts although the actual structural differences between the conformers were small (of the order of 0.1–0.2 Å). Nevertheless, this treatment generally resulted in a better agreement of the model with expected stereochemistry, as strain in the transition region between single and multiple conformations was minimized.

At the end of refinement, the best model as obtained from refinement against the working set of reflections was refined against all data for ten cycles using conjugate-gradient minimization and an $R1$ of 10.29 was obtained for all data. For the final parameterization, the entire normal matrix was inverted after removal of all restraints. The inversion of the matrix corresponding to 7433 parameters refined against 41 006 reflections ran in 148 MB of memory and took 33 min of CPU time on an Intel P4 processor running at 2.2 GHz under Linux 2.4.4.

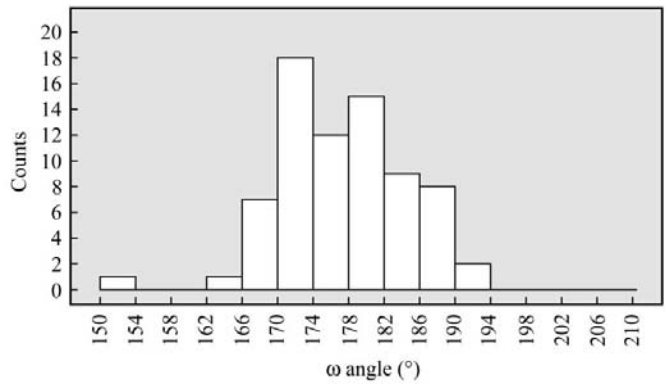

Figure 1
Histogram of ω angles in the atomic resolution structure of tendamistat.

2.4. Comparison of models

To compare the two models of tendamistat alone (PDB codes 1hoe and 1ok0) and tendamistat in complex with pig pancreatic α-amylase, error-scaled difference distance matrices (Schneider, 2002) were calculated for C^α atoms of residues 4–74 between the different conformations. The percentage of matrix elements smaller than 2.0σ was found to be between 99.6 and 100.0%, indicating that in terms of their backbone conformation all models are identical within error (Schneider, 2002).

The overall r.m.s.d.s after least-squares superposition (Kabsch, 1976) of C^α atoms 4–74 from 1ok0 and 1hoe, and from 1ok0 and tendamistat from 1bvn are 0.21 and 0.43 Å, respectively.

3. Results and discussion

3.1. Quality of the model

Of the 558 non-H atoms in tendamistat, 463 were modeled in fully occupied single sites and the remaining 95 atoms were described by two discrete partially occupied conformations. In addition to the protein, 76 fully and 83 partially occupied water molecules, two glycerol molecules and a Cl^- ion in two positions have been included in the model. All non-glycine and non-proline residues display main-chain dihedral angles that fall within the allowed (95.2%) or the additionally allowed (4.8%) region of the Ramachandran plot as defined by the program *PROCHECK* (Laskowski *et al.*, 1993). The ω angles show a broad distribution centred around 177.4° (Fig. 1), whilst the ω angle between residues Tyr20 and Ser21 shows a very extreme value of 153.2° with a standard uncertainty of 0.7° as measured by inversion of the full normal matrix of the refinement. The low standard uncertainty for this angle plus the fact that all atoms involved have well defined electron density (Fig. 2) and B values smaller than 5.5 Å^2 show that this distortion from a planar arrangement by almost 30° is a valid observation.

The coordinate uncertainties for fully occupied atoms are mostly smaller than 0.04 Å and show a strong correlation with the B values and the type of the respective atoms (Fig. 3*a*) as described previously (Cruickshank, 1999). For partially occupied protein atoms, the estimates for the coordinate uncertainties are on average larger and span a much wider range than for fully occupied protein atoms (Fig. 3*b*). Particularly large coordinate uncertainties are observed for partially occupied sites which have another partially occupied site in the immediate vicinity (Fig. 3*b*). Such cases correspond to situations where two sites effectively share the same electron density. For the calculation of realistic coordinate uncertainties for these sites, the common approach of inverting the unrestrained full matrix may not be appropriate

because for sites sharing the same electron density the extra information conferred by restraints is necessary to obtain a well defined set of parameters.

3.2. Overall structure

Tendamistat has an immunoglobulin-like fold consisting of two three-stranded antiparallel β-sheets stabilized by two disulfide bridges (Fig. 4*a*). A prominent feature is the triplet of Trp18, Arg19 and Tyr20 located between the first and the second β-strand. The side chains of these three residues, which are conserved in this class of inhibitors (Vértesy & Tripier, 1985), are stacked on top of each other and form key interactions in the complex with pig pancreatic α-amylase (Wiegand *et al.*, 1995).

The other two crystallographic models of tendamistat available from the PDB are the original structure at room temperature determined at a resolution of 2.0 Å (Pflugrath *et al.*, 1986) and the complex between tendamistat and pig pancreatic α-amylase determined at 2.5 Å (Wiegand *et al.*, 1995). With respect to the backbone conformation of residues 4–74, all three models are identical within error (see §2). The absence of large conformational differences is interesting from the point of view that the current structure and 1hoe are uncomplexed molecules for which crystals were grown at rather extreme pH values of below 1.6, whereas the structure of the complex (1bvn) was determined at a pH of 9.0. This observation is consistent with the pH-independence of the enzyme inhibition (Vértesy *et al.*, 1984), which may be important for *S. tendae* in order to make use of tendamistat in an environment of varying pH as found in the vicinity of other acid-producing microorganisms. Furthermore, the stability of tendamistat at very acidic pH is of advantage with respect to its application in the human stomach.

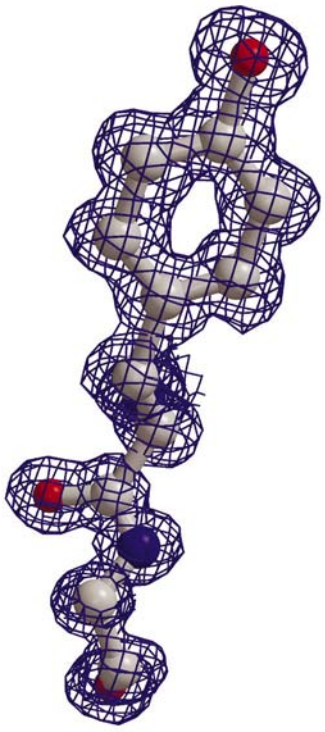

Figure 2
$2F_o - F_c$ electron-density map around residues Tyr20 and Ser21 contoured at 1.0σ. The carboxyl group of Ser21 is left out for clarity. The figure was prepared with *BOBSCRIPT* (Kraulis, 1991; Esnouf, 1999).

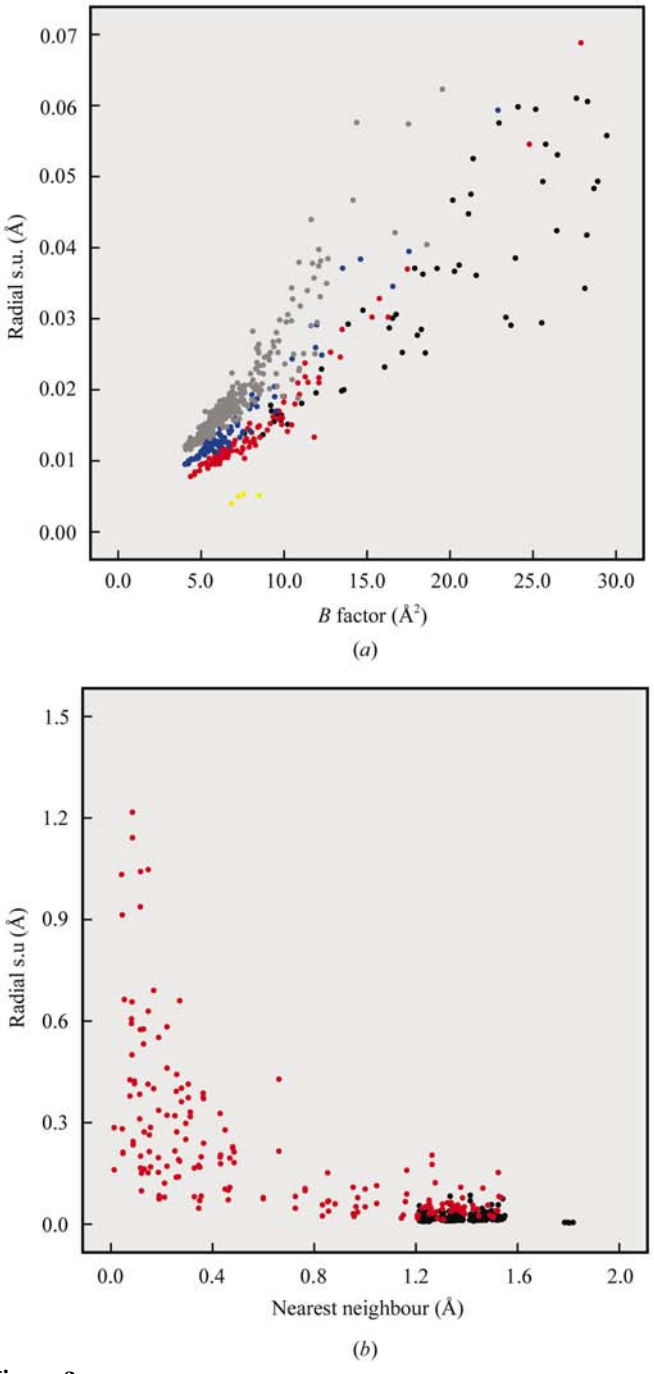

Figure 3
(*a*) Scatter plot of radial coordinate uncertainty *versus* equivalent isotropic *B* factor for fully occupied atoms. Black dots represent water molecules; grey, blue, red and yellow indicate C, N, O and S atoms belonging to the protein. (*b*) Scatter plot of radial coordinate uncertainty *versus* distance to the nearest other site for fully (black) and partially (red) occupied protein sites.

Table 3
Residues modelled in more than one conformation.

For residues located in clusters of disorder, Cn indicates the number of the cluster and '—' denotes isolated patches of disorder. 'Occ' gives the occupancy of the major conformation and 'Atoms' lists the atoms with non-unit occupancy. For crystal contacts, residue numbers of residues related by crystal symmetry for which at least one atom is closer than 3.5 Å to a disordered atom are listed.

Res	Cn	Occ	Atoms	Crystal contacts
Asp1	—	0.59	All	Leu74
Thr3	—	0.77	All	Trp18, Arg19, Gly26
Glu6	II	0.51	C^{δ}, $C^{\varepsilon1}$, $C^{\varepsilon2}$	Ile61
Pro7	—	0.72	C^{β}, C^{γ}, C^{δ}	Arg18
Pro9	II	0.51	C^{β}, C^{γ}	None
Thr13	I	0.62	All	None
Tyr15	I	0.62	All	None
Asp24	I	0.62	C^{β}, C^{γ}, $C^{\delta1}$, $C^{\delta2}$	Tyr20
Glu29	II	0.51	All	None
Thr30	II	0.51	All	None
Val31	II	0.51	All	None
Val35	—	0.61	All	None
Ile53	I	0.62	All	Gly57, Asp58
Thr54	I	0.62	All	None
Thr55	I	0.62	N	None
Arg72	I	0.62	All	None

3.3. Multiple conformations

The diffraction data to atomic resolution support the modelling of a number of atoms in multiple conformations. These multiple conformations in fact represent the largest differences from the previously determined structures. The 95 protein atoms modelled in two discrete sites correspond to ∼17% of all non-H atoms in the protein and can be grouped into two large networks and several isolated patches (Table 3). Several disordered regions are in contact with symmetry-related molecules; the atoms in the contacted molecule are always ordered (Table 3).

The first network of disordered residues consists of Thr13, Tyr15, Asp24, Ile53, Thr54 and Thr55 (occupancies of 62 and 38%) and is located in the β-sheet region on the side of tendamistat involved in the binding to α-amylase. For the side chain of residue Tyr15, which is found in two well defined conformations whose main difference is a difference of 137° in the χ_1 torsion angle, no electron density was present in the previous X-ray study at room temperature (Pflugrath *et al.*, 1986). These newly observed conformations document the advantage of atomic resolution crystallography with respect to crystallography at medium resolution for the identification of partially occupied sites. In the NMR model (Kline *et al.*, 1988), the side chain of Tyr15 is defined by 26 NMR distance constraints and shows a single χ_1 torsion angle of 128 ± 14°, which is between the two values observed in the present structure (−61 and 161°). Given the fact that in the present crystal structure both conformers of Tyr15 are within 4.5 Å of atoms belonging to a neighbouring molecule in the crystal lattice, the NMR conformation may correspond to the actual conformation in solution, whilst the conformations observed in the crystal represent

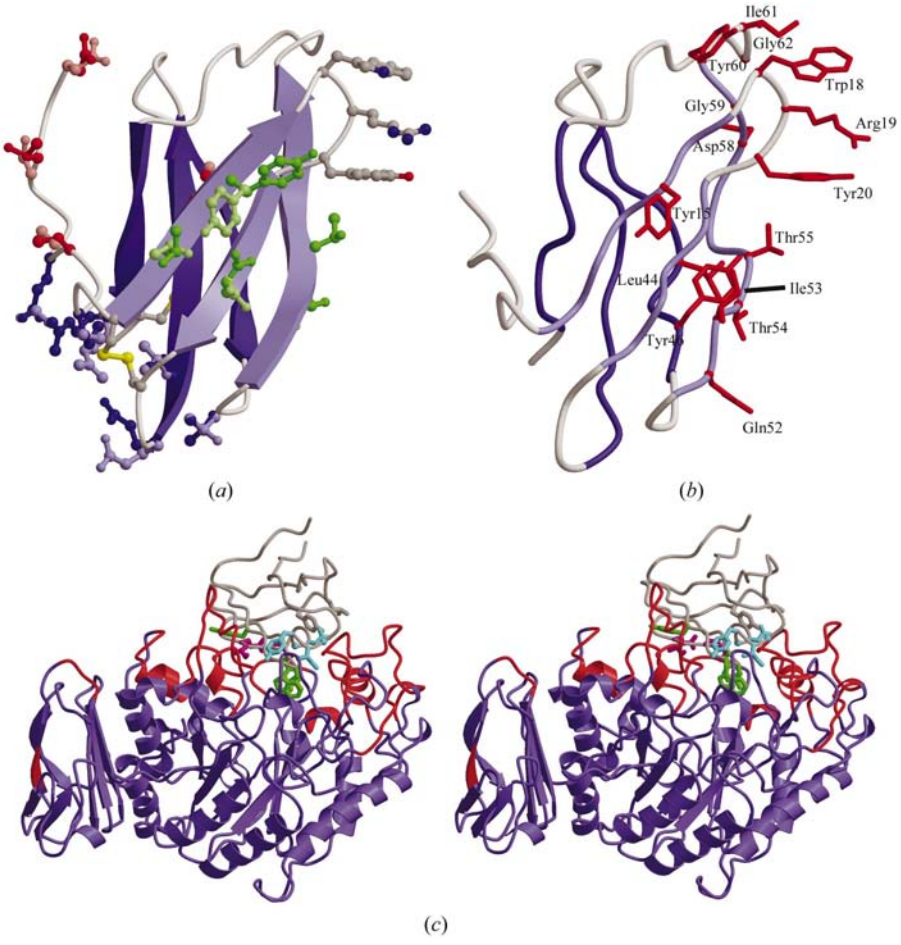

Figure 4
(*a*) Schematic view of the atomic resolution model of tendamistat. β-Strands are shown in blue and disulfide bridges in yellow. Side chains of residues modelled in two conformations are shown in ball-and-stick representation in different colours, where light and dark colours indicate the different conformations. The first cluster (Thr13, Tyr15, Asp24, Ile53, Thr54, Thr55) is shown in green and the second cluster (Glu6, Pro9, Glu29, Thr30, Val31, Arg72) in blue; isolated disordered residues are indicated in red. (*b*) Schematic view of the structure of tendamistat in the complex with pig-pancreatic α-amylase (Wiegand *et al.*, 1995). β-Strands are indicated in blue and side chains of residues involved in binding the target molecule are shown in red. (*c*) Stereoview (cross-eyed) of the complex between pig pancreatic α-amylase (blue and red) and tendamistat (Wiegand *et al.*, 1995) (grey). Parts of the enzyme that were identified as conformationally invariant by comparison of seven conformers (Schneider, 2002) are shown in blue and flexible regions are shown in red. For tendamistat, side chains of residues involved in binding to α-amylase are shown in green, grey, magenta and cyan for segments 1–4, respectively. For a definition of the segments see §3.4 of the text. All figures were prepared with *MOLSCRIPT* (Kraulis, 1991).

Table 4
Different degrees of ordering for residues involved in the binding between tendamistat and pig pancreatic α-amylase in different structural models.

'Seg' stands for the segments as defined in the text. Average *B* values for side chains of residues involved in the binding in the two crystal structures of tendamistat alone (1hoe, 1ok0) and in complex with pig pancreatic α-amylase (1hoe) are given. For residues modelled in two conformations, the *B* values are printed in bold. For the NMR structure, the averaged displacements within the NMR ensemble as given in Fig. 2 in Billeter *et al.* (1989) are listed and average displacements larger than 1.5 Å are printed in bold. Names of residues that show signs of flexibility in at least one of the structure determinations are printed in bold. For crystal contacts, residue numbers of residues related by crystal symmetry for which at least one atom is closer than 3.5 Å to a residue involved in α-amylase binding are listed.

		B value (Å)				
Seg	Residue	1hoe	1ok0	1bvn	R.m.s.d. NMR	Crystal contacts in 1ok0
	All	20.9 ± 14.0	8.9 ± 3.9	30.3 ± 9.2		
1	**Tyr15**	**Not obs.**	**9.4 ± 2.9**	26.9 ± 3.0	0.8	None
	Trp18	9.7 ± 3.7	5.1 ± 0.2	31.4 ± 2.7	**1.9**	Val27
	Arg19	15.5 ± 10.5	5.8 ± 1.1	21.7 ± 2.8	**4.0**	Gly26, Gly51, Cys345
	Tyr20	14.8 ± 5.4	7.8 ± 1.1	20.4 ± 3.0	**3.2**	Asp24
2	Leu44	16.8 ± 2.7	7.6 ± 1.5	35.5 ± 1.2	1.1	Gln22
	Tyr46	19.6 ± 6.6	6.0 ± 0.4	19.9 ± 2.6	1.2	Gln22, Ile53
3	Gln52	41.2 ± 15.2	11.1 ± 3.5	34.7 ± 0.5	1.4	Asp58
	Ile53	14.8 ± 3.5	**8.7 ± 3.4**	31.5 ± 1.8	0.8	Tyr46, Gly57, Asp58
	Thr54	27.9 ± 3.8	**8.4 ± 3.0**	31.9 ± 4.9	0.7	None
	Thr55	6.7 ± 3.5	**7.0 ± 0.7**	28.6 ± 2.8	0.9	None
4	**Asp58**	14.1 ± 3.0	7.4 ± 3.3	30.4 ± 6.6	**4.0**	Gly51, Gln52, Ile53
	Gly59	n/a	n/a	n/a	n/a	Gly51
	Tyr60	16.1 ± 3.9	10.0 ± 2.5	21.0 ± 1.6	**1.8**	None
	Ile61	14.9 ± 7.3	7.1 ± 1.0	18.7 ± 0.6	**1.9**	Val50
	Gly62	n/a	n/a	n/a	n/a	None

conformations that become populated when tendamistat interacts with another molecule. In fact, the conformation assumed by Tyr15 in the complex with pig pancreatic α-amylase shows a χ_1 torsion angle of −68°, corresponding to the minor conformation observed here.

The second cluster contains residues located in parts of the chain that are not stabilized by secondary-structure elements: Glu6, Pro9, Glu29, Thr30, Val31 and Arg72 (both conformers with refined occupancies of 50%). Four more residues (Thr3, Pro7, Val35 and Asp1) exhibit multiple conformers isolated from larger networks.

3.4. Residues involved in target binding

The determination of the crystal structure of the complex between pig pancreatic α-amylase and tendamistat by Wiegand *et al.* (1995) showed that about 30% of the water-accessible surface of the inhibitor is in contact with the target molecule. The contacts between the enzyme and the inhibitor comprise four segments of the polypeptide chain of tendamistat and involve a total of 15 residues (Fig. 4*b*): Tyr15, Trp18, Arg19 and Tyr20 in segment 1; Leu44 and Tyr46 in segment 2; Gln52, Ile53, Thr54 and Thr55 in segment 3; Asp58, Gly59, Tyr60, Ile61 and Gly62 in segment 4. When tendamistat is bound to pig pancreatic α-amylase, all these residues are well ordered as indicated by their average *B* values (Table 4). However, for the uncomplexed form of tendamistat, varying degrees of flexibility are seen in the different models originating from X-ray diffraction and NMR experiments.

In segment 1, the first residue displaying flexibility in the uncomplexed form is the aforementioned Tyr15. This residue has been been suggested to play an important role in the strong interaction between tendamistat and mammalian amylases, as it interacts with the glycine-rich insertion (residues His305-Gly306-Ala307-Gly308-Gly309-Ser310 in pig pancreatic α-amylase) found in these enzymes (Machius *et al.*, 1996). The fact that the glycine-rich insertion undergoes large conformational changes of the order of 3–4 Å when different ligands, *e.g.* acarbose (Gilles *et al.*, 1996), an inhibitor from bean (Bompard-Gilles *et al.*, 1996) or a substrate analogue (Qian *et al.*, 1997), are bound shows that this loop has considerable mobility. Thus, complementary flexibility may be necessary on the side of the inhibitor in order to achieve the best possible binding.

The triplet containing residues 18–20 is found to be mobile in the NMR ensemble and well ordered in the complex with pig pancreatic α-amylase. The present structure shows low average *B* values for the side chains of Trp18 and Arg19 and slightly elevated *B* values for Tyr20. However, the single conformation of this group of residues seen here may be imposed by the formation of the crystal lattice as indicated by the crystal contacts listed for Trp18–Tyr20 in Table 4. In fact, the two highest peaks in the final $F_o - F_c$ difference Fourier map are located in the region of Tyr20, indicating a possible weak second conformation for this residue.

For segment 3, all atoms are well defined in the NMR structure, whereas in the atomic resolution crystal structure almost all residues are present in double conformations. The disordered parts of Ile53–Thr55 are in fact connected to Tyr15 by means of interpenetrating networks of multiple conformations that are mutually exclusive owing to steric clashes.

The residues belonging to segment 4 (Arg58–Gly62) are stabilized in a single conformation in the crystal form that was used for the determination for both the 2.0 Å and the 0.93 Å resolution structure. This stabilization is affected by intermolecular hydrogen bonds between Asp58 $O^{\delta 2}$ and and a symmetry-related Ile53 N (3.03 Å) and between Gly59 N and a symmetry-related Gly51 N (2.87 Å) and by a van der Waals interaction between Ile61 $C^{\gamma 2}$ (3.30 Å) and Pro50 O of the neighbouring molecule. For this region, the NMR ensemble, as one would expect for a surface loop containing two glycine residues, indicates a higher flexibility.

4. Conclusions

The crystal structure of tendamistat has been determined to 0.93 Å resolution. At this resolution, 95 atoms of the 558 atoms present in the protein molecule were modelled in two discrete conformations. The final model has an average co-

ordinate uncertainty for fully occupied sites of 0.018 Å. This very detailed and precise model together with the standard uncertainties for all parameters derived from a full-matrix inversion provides a firm basis for future theoretical studies.

It was found that partially occupied sites showed substantially larger and frequently grossly overestimated coordinate uncertainties than fully occupied sites. For such sites, the error estimates obtained from unrestrained full-matrix inversion may be misleading as they do not reflect the precision of the restrained model. However, for a restrained model the coordinate uncertainties will depend on the relative weighting between X-ray and restraint terms in the target function of the refinement. The influence of different weighting schemes on the uncertainties of model parameters will be the subject of future work.

The multiple conformations detected in the electron-density maps at atomic resolution complement the information about the flexibility of tendamistat previously derived from an NMR study in solution (Kline *et al.*, 1988). Some regions found to be rigid in the NMR study were modelled in the crystal structure as two conformations possibly stabilized by interactions with neighbouring molecules in the crystal lattice.

Of particular interest are the residues of tendamistat that interact with α-amylase upon complex formation. For most of these residues, the crystallographic and NMR experiments provide complementary evidence for their conformational variability. On one hand, the flexibility of the inhibitor could implement a conformational repertoire used to achieve a broad target specificity. On the other hand, the mobility of the atoms involved in the interaction between tendamistat and pig pancreatic α-amylase allows optimization of the binding by conformational adjustments. In fact, as found previously from a comparison of seven different models of the enzyme (Schneider, 2002), the active-site region of pig pancreatic α-amylase itself contains several mobile regions (Fig. 4*c*) also providing adjustability on the side of the enzyme. From the experimental point of view, an induced-fit type of binding mode involving conformational rearrangements of both partners is supported by the observation that the binding of tendamistat to pig pancreatic α-amylase is slow and progressive (Vértesy *et al.*, 1984). Consequently, the flexibility of the binding regions of tendamistat may be considered as an interesting parameter in the design of new α-amylase inhibitors.

We are grateful to Elspeth Garman for pointing out the usefulness of acupuncture needles for crystal surgery and to George M. Sheldrick for helpful discussions.

References

Aschauer, H., Vértesy, L., Nesemann, G. & Braunitzer, G. (1983). *Hoppe-Seyler's Z. Physiol. Chem.* **364**, 1347–1356.

Bachmann, A. & Kiefhaber, T. (2001). *J. Mol. Biol.* **306**, 375–386.

Balbach, J., Seip, S., Kessler, H., Scharf, M., Kashani-Poor, N. & Engels, J. W. (1998). *Proteins*, **33**, 285–294.

Billeter, M., Kline, A. D., Braun, W., Huber, R. & Wüthrich, K. (1989). *J. Mol. Biol.* **206**, 677–687.

Bompard-Gilles, C., Rousseau, P., Rouge, P. & Payan, F. (1996). *Structure*, **4**, 1441–1452.

Bonvin, A. M. & van Gunsteren, W. F. (2000). *J. Mol. Biol.* **296**, 255–268.

Braun, W., Epp, O., Wüthrich, K. & Huber, R. (1989). *J. Mol. Biol.* **206**, 669–676.

Cruickshank, D. W. J. (1999). *Acta Cryst.* D**55**, 583–601.

Doruker, P., Atilgan, A. R. & Bahar, I. (2000). *Proteins*, **40**, 512–524.

Esnouf, R. M. (1999). *Acta Cryst.* D**55**, 938–940.

Gilles, C., Astier, J. P., Marchis-Mouren, G., Cambillau, C. & Payan, F. (1996). *Eur. J. Biochem.* **238**, 562–559.

Gorler, A. & Kalbitzer, H. R. (1997). *J. Magn. Reson.* **124**, 177–188.

Kabsch, W. (1976). *Acta Cryst.* A**32**, 922–923.

Kline, A. D., Braun, W. & Wüthrich, K. (1988). *J. Mol. Biol.* **204**, 675–724.

Kottke, T. & Stalke, D. (1993). *J. Appl. Cryst.* **26**, 615–619.

Kraulis, P. J. (1991). *J. Appl. Cryst.* **24**, 946–950.

Laskowski, R. A., MacArthur, M. W., Moss, D. S. & Thornton, J. M. (1993). *J. Appl. Cryst.* **26**, 283–291.

McRee, D. E. (1999). *J. Struct. Biol.* **125**, 156–165.

Machius, M., Vértesy, L., Huber, R. & Wiegand, G. (1996). *J. Mol. Biol.* **260**, 409–421.

Meyer, B. H., Muller, F. O., Kruger, J. B. & Grigoleit, H. G. (1984). *S. Afr. Med. J.* **65**, 287–288.

Ono, S., Umezaki, M., Tojo, N., Hashimoto, S., Taniyama, H., Kaneko, T., Fujii, T., Morita, H., Shimasaki, C., Yamazaki, I., Yoshimura, T. & Kato, T. (2001). *J. Biochemistry*, **129**, 783–790.

Otwinowski, Z. & Minor, W. (1997). *Methods Enzymol.* **276**, 307–326.

Pappenberger, G., Aygün, H., Bachmann, A., Müller, R., Engels, J. W. & Kiefhaber, T. (2003). *J. Mol. Biol.* **326**, 235–246.

Pappenberger, G., Saudan, C., Becker, M., Merbach, A. E. & Kiefhaber, T. (2000). *Proc. Natl Acad. Sci. USA*, **97**, 17–22.

Pflugrath, J. W., Wiegand, G., Huber, R. & Vértesy, L. (1986). *J. Mol. Biol.* **189**, 383–386.

Qian, M., Spinelli, S., Driguez, H. & Payan, F. (1997). *Protein Sci.* **6**, 2285–2296.

Scarselli, M., Bernini, A., Segoni, C., Molinari, H., Esposito, G., Lesk, A. M., Laschi, F., Temussi, P. & Niccolai, N. (1999). *J. Biomol. NMR*, **15**, 125–133.

Schneider, T. R. (2002). *Acta Cryst.* D**58**, 195–208.

Schonbrunner, N., Pappenberger, G., Scharf, M., Engels, J. & Kiefhaber, T. (1997). *Biochemistry*, **36**, 9057–9065.

Sefler, A. M., Kozlowski, M. C., Guo, T. & Bartlett, P. A. (1997). *J. Org. Chem.* **62**, 93–102.

Sheldrick, G. M. & Schneider, T. R. (1997). *Methods Enzymol.* **277**, 319–343.

Vértesy, L., Oeding, V., Bender, R., Zepf, K. & Nesemann, G. (1984). *Eur. J. Biochem.* **141**, 505–512.

Vértesy, L. & Tripier, D. (1985). *FEBS Lett.* **185**, 187–190.

Wiegand, G., Epp, O. & Huber, R. (1995). *J. Mol. Biol.* **247**, 99–110.